American Mineralogist, Volume 92, pages 1225–1231, 2007

Galaxite, $MnAl_2O_4$, a spectroscopic standard for tetrahedrally coordinated Mn^{2+} in oxygen-based mineral structures

Ulf Hålenius,* Ferdinando Bosi, and Henrik Skogby

Department of Mineralogy, Swedish Museum of Natural History, P.O. Box 50007, SE-104 05 Stockholm, Sweden

Abstract

Chemical analyses, crystal structure refinement, cation order determination, and single-crystal optical absorption spectrum of synthetic galaxite are presented. New optical absorption spectra of natural Mn-bearing willemite, rhodochrosite, Mn-rich forsterite, and tephroite are reported for comparative purposes.

The structure of a synthetic galaxite end-member is characterized by a relatively large unit-cell edge, a_0 = 8.2104(3) Å, a *u*-parameter equal to 0.26588(7), a T-O distance of 2.0034(6) Å, and an M-O distance of 1.9310(5) Å. Mn^{2+} is strongly ordered at the tetrahedral T-site as demonstrated by the refined structural formula $^{T}(Mn^{2+}_{0.90}Al_{0.10})^{M}(Mn^{2+}_{0.10}Al_{1.90})O_4$.

The optical absorption spectrum of galaxite in the range 300–800 nm shows a set of five relatively sharp bands at 20 300, 22 250, 23 390, 25 970, and 27 780 cm^{-1} marking spin-forbidden transitions in Mn^{2+} at the tetrahedral site. The molar absorption coefficient of the field-independent $^6A_1(S) \rightarrow {}^4E_g^4A_{1g}(G)$ absorption band at 23 390 cm^{-1} equals 1.90 L/(mol·cm), which is approximately an order of magnitude higher than for corresponding bands in spectra of compounds that contain isolated Mn^{2+}-centered octahedra.

The calculated crystal field splitting, 10Dq, for Mn^{2+} at the T-site in galaxite equals 5290 cm^{-1}. This compares well with derived 10Dq-values of 5860 and 5510 cm^{-1} for Mn^{2+} at the tetrahedral T1- and T2-site in Mn-bearing willemite. In agreement with theory, the 10Dq for Mn^{2+} in MnO_4 tetrahedra is ca. 30% smaller than corresponding values in MnO_6 octahedra. The lower Racah B-parameters of the spectroscopic data indicate that the degree of covalency of Mn^{2+}-O bonds is higher in tetrahedra than in octahedra.

Keywords: Crystal structure, galaxite, optical spectroscopy, willemite, tephroite, forsterite

Introduction

Manganese, like iron, is a geochemically important element occurring as divalent, trivalent, and tetravalent cations at differently coordinated sites in common silicate and oxide minerals. Methods to distinguish the valence state and coordination of transition elements in mineral structures are essential for many branches of the earth sciences. Optical absorption spectroscopy is one of several methods that have the capability to extract such information at high spatial resolution.

The optical-absorption spectra of Fe^{2+} and Fe^{3+} in four-, five-, and sixfold coordination in minerals have been explored extensively (e.g., Rossman and Taran 2001; Taran and Langer 2001; Waychunas and Rossman 1983), but comparable data for manganese show some omissions. Many optical spectra of Mn^{2+}- and Mn^{3+}-bearing minerals have been published during the last four decades, but complete optical spectra of manganese at tetrahedral sites in oxygen-based mineral structures have not been reported. In addition to this, the vast majority of the published spectra deals with mineral structures in which Mn^{2+} is distributed at high concentrations over several sites that show different mean Mn-O bond lengths and variable distortion from octahedral symmetry. In fact, presence of several non-equivalent Mn-centered sites is characteristic for all the silicate minerals containing MnO_6-clusters, which are included in the comprehensive list of spectroscopic data on Mn^{2+}-bearing minerals presented by Burns (1993). This structural complexity makes spectral band assignments difficult. Consequently, published parameters (e.g., crystal field splitting and Racah) on Mn^{2+} at octahedral sites in minerals derived from optical absorption spectra must be regarded with some caution.

For these reasons we present in this paper optical absorption spectra of Mn^{2+} in tetrahedral oxygen coordination in spinel (galaxite) and phenacite (willemite) group minerals. To relate the spectra of divalent manganese at tetrahedral sites with those of MnO_6^{10-}-cluster we have recorded spectra of three structurally simple minerals; Mn-rich forsterite, tephroite, and rhodochrosite at relatively high spectral resolution.

Samples and methods

Synthetic galaxite

Single crystals of end-member galaxite, $MnAl_2O_4$, were synthesized by use of a flux-growth method. Nutrient components

* E-mail: ulf.halenius@nrm.se

0003-004X/07/0007–1225$05.00/DOI: 10.2138/am.2007.2481

were weighed out in pre-dried oxide form (analytical grade) with a surplus of Al_2O_3 to minimize potential stabilization of trivalent manganese in the products. The nutrient oxides were mixed with $Na_2B_4O_7$ acting as flux compound, using a flux/oxide ratio of 0.8, and were homogenized under acetone in an agate mortar. Approximately 7 g of the mixture was placed in a 12 cc crucible of yttria-stabilized Pt/Au(5%), covered by a lid, and placed in a vertical furnace equipped with Tylan CO_2:H_2 flow controllers. A continuous flow of the two gases in the ratio 1:2 was adopted to obtain oxygen fugacity ranging from 10^{-12} to 10^{-17} bars when the temperature was varied from 1200 to 900 °C. Thermal runs consisted of an initial increase to 1200 °C where the temperature was kept constant for 24 h to allow for complete dissolution of the oxides and melt homogenization. Subsequently, the temperature was decreased by 4 °C/h to 900 °C, followed by a fast cooling down to ambient temperature. The synthesis product consisted of yellow-colored galaxite and colorless corundum crystals dispersed in sodium borate glass. The glass was dissolved in a warm diluted HCl solution.

Natural samples

Single crystals of Mn-bearing willemite ($[Zn, Mn]_2SiO_4$), Mn-rich forsterite ($[Mg, Mn]_2SiO_4$), tephroite (Mn_2SiO_4), and rhodochrosite ($MnCO_3$) were selected from specimens in the mineral collections at the Swedish Museum of Natural History. Information on provenience and collection numbers of these specimens is summarized in Table 1. Single crystal absorbers of these optically anisotropic minerals were prepared from euhedral grains oriented with the aid of crystal morphology and optical microscopy utilizing conoscopic interference figures.

Electron microprobe analysis

Electron microprobe analysis of the present samples were obtained with a Cameca SX50 instrument at the University of Uppsala operating at an accelerating potential of 15 kV and a sample current of 12 nA. Standard samples were synthetic Al_2O_3 (for Al), MgO (Mg), $CaSiO_3$ (Ca and Si), $MnTiO_3$ (Mn and Ti), Fe_2O_3 (Fe), ZnS (Zn), and natural albite (Na), orthoclase (K), and vanadinite (Pb). For raw data reduction, the PAP computer program was applied (Pouchou and Pichoir 1984). The results are summarized in Table 1.

Single-crystal structural refinement

A single crystal (ca. 250 × 250 × 250 μm) of synthetic galaxite was mounted on a Siemens P4 automated four-circle, single-crystal diffractometer. Details of the data collection are summarized in Table 2. For collection of diffraction intensity data, one-eighth of the reciprocal space was examined with the ω scan method at a fixed scan range. The scan speed was variable, depending on reflection intensity, as estimated through pre-scans. The background was measured with a stationary counter and crystal at the beginning and end of each scan, in both cases for half the scan time. Three standard reflections were monitored every 47 measurements. Further details of the experimental conditions can be found in Lucchesi et al. (1997).

The SHELXTL-PC program package was used for reduction of X-ray diffraction data. Intensities were corrected for polarization and Lorentz effects. Absorption corrections were accomplished with a semi-empirical method (North et al. 1968). All reflections were used in the refinement. No significant deviations from $Fd\bar{3}m$ symmetry were noted. Appearance of forbidden space-group reflections such as (200) was attributed, on the basis of ψ-scan checks, to double reflection (Tokonami and Horiuchi 1980). Variable parameters during the structural refinement were scale factor, oxygen coordinate, mean atomic number of tetrahedral (T) and octahedral (M) sites, displacement parameters, and isotropic secondary extinction coefficients. The starting oxygen coordinate proposed by Lucchesi et al. (1997), setting the origin at $\bar{3}m$, was used. No chemical constraints were applied during the refinement. Partially ionized (for O and ^{M}Al) and fully ionized (for $^{T}Mn^{2+}$) scattering curves were applied as these resulted, as observed by Della Giusta et al. (1996), in the best conventional agreement factors over all sinθ/λ intervals and the best correspondence between observed and calculated F(222). Off-diagonal displacement parameters were extremely small and of the same magnitude as their standard deviation, when not forced to zero by symmetry. Three isotropic, full-matrix, refinement cycles were followed by anisotropic cycles until convergence was attained. No significant correlation ($r^2 < 0.40$) between parameters was observed

Optical absorption spectroscopy

Optical absorption spectra in the UV/VIS range, 300–800 nm (33 333 to 12 500 cm^{-1}), were recorded at room temperature on double-sided polished single crystals of high optical quality. The absorber thickness of the studied minerals was 103 (galaxite), 206 (tephroite), 389 (Mn-rich forsterite), 415 (rhodochrosite), and 893 μm (willemite). Spectra were recorded with a Zeiss MPM800 single beam microscope-spectrometer using Zeiss Ultrafluar 10× lenses as condenser and objective. A 75W Xenon arc lamp served as a light source and a photomultiplier as detector. Polarized spectra of the aniostropic phases were recorded using a Glan-Thompson prism. The accuracy of wavelength and absorbance readings of the spectrometer was

Table 1. Sample origin and composition

Mineral	Galaxite	Willemite	Forsterite	Tephroite	Rhodochrosite
Locality	Synthetic	Franklin, NJ, U.S.A.	Långban, Sweden	Franklin, NJ, U.S.A.	CO, U.S.A.
Collection no.		NRM no. 333857	NRM no. 15934	NRM no. 24308	NRM no. 881868
SiO_2 (wt%)	nd	27.06	34.94	29.30	nd
Al_2O_3	58.73	nd	0.03	0.00	nd
TiO_2	nd	nd	nd	nd	nd
MgO	nd	0.18	25.14	0.43	0.67
CaO	nd	nd	0.23	0.66	0.15
MnO	41.35	6.64	38.66	67.65	60.24
FeO	nd	nd	0.05	0.03	0.05
ZnO	nd	66.72	0.12	1.59	0.02
PbO	nd	nd	nd	nd	0.41
CO_{2calc}					38.27
SUM	100.08	100.60	99.16	99.66	99.81
Formula based on 3 cations (galaxite, willemite, forsterite, and tephroite) and 1 cation (rhodochrosite)					
Si (apfu)	nd	0.987	0.993	0.986	nd
Al	1.992	nd	0.001	0.000	nd
Ti	nd	nd	nd	nd	nd
Mg	nd	0.010	1.065	0.022	0.019
Ca	nd	nd	0.007	0.024	0.003
Mn	1.008	0.205	0.930	1.928	0.976
Fe	nd	nd	0.001	0.001	0.001
Zn	nd	1.797	0.002	0.040	0.000
Pb	nd	nd	nd	nd	0.001

Notes: nd = not detected. Estimated relative errors for major elements are ±1% in all analyses.

monitored by recording spectra of Ho_2O_3-doped and Pr_2O_3/Nd_2O_3-doped calibration standards (Hellma glass filters 666-F1 and 666-F7). Sample spectra were recorded during three collection cycles in 0.5 nm steps at a spectral resolution of 1 nm. Air served as a reference medium in all measurements. The diameter of the measuring spot equaled 50 μm. To define band positions and intensities, fits of the recorded spectra were performed with the Jandel PeakFit software under the assumption of Gaussian peak shapes. The precision of the energies (positions) of the field-independent absorption bands is estimated to be better than 60 cm^{-1}.

Results

Crystal chemistry

The chemical analyses of our synthetic galaxite show, within analytical errors, an ideal $MnAl_2O_4$ end-member composition (Table 1). The result of the structural refinement of this galaxite is summarized in Table 3. On the basis of scattering powers at the T and M sites, the following structural formula was refined: $^{T}(Mn^{2+}_{0.90}Al_{0.10})^{M}(Mn^{2+}_{0.10}Al_{1.90})O_4$. This cation distribution explains why the observed tetrahedral (2.003 Å) and octahedral (1.931 Å) bond distances differ from the optimized bond distances of $^{T}Mn^{2+}$ (2.036 Å) and ^{M}Al (1.908 Å) in spinel group minerals (Lavina et al. 2002). In our sample, disordering of Mn^{2+} and Al over the T and M site equals 0.10 apfu. This value is much lower than 0.29–0.34 apfu reported by Greenwald et al. (1954) for synthetic galaxite. However, it is comparable with $^{M}Mn^{2+}$ and ^{T}Al contents in natural galaxites reported by Lucchesi et al. (1997) and Essene and Peacor (1983), respectively.

Chemical analyses (Table 1) of the Mn-bearing willemite shows a Mn^{2+} content equal to 0.21 apfu, which may be disordered over the two irregular non-equivalent tetrahedra T1 and T2 (Sreekanth Chakradhar et al. 2004). Mn-rich forsterite shows comparable contents of Mn^{2+} (0.93 apfu) and Mg (1.07 apfu). As demonstrated by Francis and Ribbe (1980), Mn^{2+} orders strongly at the larger octahedral site (M2), while the Mg occupies the other non-equivalent octahedron (M1). In our tephroite, the Mn^{2+} content is 1.93 apfu, which is expected to result in comparable Mn^{2+} occupancies at the M1 and M2 octahedra. The chemical analyses of our rhodochrosite sample show a nearly complete Mn^{2+} occupancy (0.98 apfu) at the octahedral M-site.

Table 2. Parameters for X-ray data collection

Determination of unit-cell parameters	
Radiation	Mo$K\alpha_1$ (0.70930 Å)
Reflections used	13 (Friedel pairs on both +2θ and −2θ)
Range	85–95 °2θ
Temperature	296 K
Diffraction intensity collection	
Radiation	Mo$K\alpha$ (0.71073 Å)
Monochromator	High crystallinity graphite crystal
Range	3–95 °2θ
Reciprocal space range	$0 \le h \le 17$; $0 \le k \le 17$; $0 \le l \le 17$
Scan method	ω
Scan range	2.4°
Scan speed	Variable 1.502–14.648 °/min
Temperature	296 K
Data reduction	
Refinement	SHELXTL-PC
Corrections	Lorentz, Polarization
Absorption correction	Semi-empirical, 13ψ scans (10–95 °2θ)
Set of measured reflections	723
Set of unique reflections	151 [$I > 2\sigma(I)$]

Table 3. Results of the structural refinement of galaxite

a_0 (Å)	8.2104(3)
u	0.26588(7)
T-O (Å)	2.0034(6)
M-O (Å)	1.9310(5)
m.a.n. T	23.81(9)
m.a.n. M	13.60(6)
U_{11} (T)	0.0060(2)
U_{11} (M)	0.0053(2)
U_{11} (O)	0.0090(2)
U_{12} (M)	−0.0004(1)
U_{12} (O)	−0.0003(2)
Ext.	0.0053(2)
R1(F) (%)	1.97

Notes: T-O and M-O = tetrahedral and octahedral bond distances, respectively. m.a.n. = mean atomic number; U_{11} = displacement parameters (Å^2); $U_{11} = U_{22} = U_{33}$ and $U_{12} = U_{13} = U_{23}$ (= 0 for the T-site due to symmetry reasons); Ext. = isotropic secondary extinction coefficient, according to Larson's algorithm (1970); R1(F) in the form: $(\Sigma||F_{obs} - F_{calc}||)/(\Sigma F_{obs})$. Space group: $Fd\bar{3}m$, $Z = 8$.

Optical absorption spectra of tetrahedrally coordinated Mn^{2+} in minerals

The optical absorption spectrum of a galaxite single crystal (Fig. 1) reveals a set of five relatively narrow absorption bands typical of spin-forbidden electronic d-d transitions, with the sharp and relatively strong field-independent d-d bands due to the $^6A_1(S) \rightarrow {}^4E_g(D)$ and $^6A_1(S) \rightarrow {}^4E_g{}^4A_{1g}(G)$ transitions in Mn^{2+} at 27 780 and 23 390 cm^{-1}, respectively. The molar absorption coefficient of the band caused by the latter transition equals 1.90 L/(mol·cm). The field-dependent transitions $^6A_1(S) \rightarrow {}^4T_{2g}(D)$, $^6A_1(S) \rightarrow {}^4T_{2g}(G)$, and $^6A_1(S) \rightarrow {}^4T_{1g}(G)$ are observed at 25 970, 22 250, and 20 300 cm^{-1}, respectively. The spectrum of our end-member galaxite is, with the exception of more intense bands due to a higher Mn-concentration, very similar to that obtained for a synthetic high-temperature spinel sensu stricto doped with low concentrations, 0.001–0.050 apfu, of Mn^{2+} (Jouini et al. 2006). However, their proposed assignments for the recorded Mn^{2+}-bands in these spectra are not reasonable as they lead to an unrealistically low Racah parameter B (≈370 cm^{-1}). Our spectrum shows no traces of Mn^{3+}, which in spinel give rise to very strong

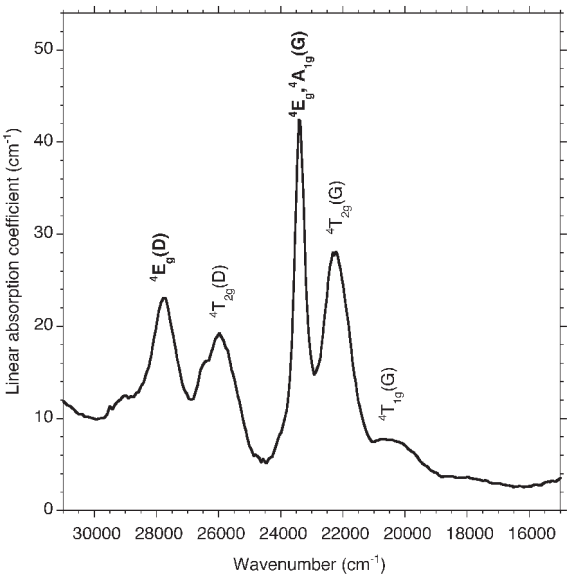

Figure 1. Optical absorption spectrum of synthetic end-member galaxite with excited state terms for each band indicated.

and broad spin-allowed d-d bands in the range 20 000–25 000 cm^{-1} (Bosi et al. 2007).

The polarized absorption spectra of willemite single crystals (Fig. 2) reveal band structures comparable to the one recorded in the galaxite spectrum. The sharp and intense field-independent $^6A_1(S) \rightarrow {}^4E_g(D)$ and $^6A_1(S) \rightarrow {}^4E_g{}^4A_{1g}(G)$ transitions in Mn^{2+} occur at 28 010 and 23 700 cm^{-1}, respectively. These bands show molar absorption coefficients of 0.80 L/(mol·cm). The bands caused by the field-dependent transitions $^6A_1(S) \rightarrow {}^4T_{2g}(D)$, $^6A_1(S) \rightarrow {}^4T_{2g}(G)$, and $^6A_1(S) \rightarrow {}^4T_{1g}(G)$ are distinctly split. This feature, which we ascribe to the fact that Mn^{2+} is distributed over two non-equivalent tetrahedral sites (e.g., Sreekanth Chakradhar et al. 2004; Patra et al. 2005), was not noted in the unpolarized partial (18 000–25 000 cm^{-1}) absorption spectrum of willemite published by Gerner et al. (2004). The assignment of the field-dependent bands is not unequivocal, but with regard to the difference in mean bond lengths of the two T-sites (Klaska et al. 1978) it is most likely that the bands at 21 230, 22 700, and 27 070 cm^{-1} are caused by Mn^{2+} at the larger T2-tetrahedron, while the bands at 20 370, 23 120, and 26 320 cm^{-1} mark transitions in Mn^{2+} at the smaller T1-tetrahedron. Alternative site assignments of these field-dependent bands yield, in view of the small size differences in bond distances for the two tetrahedra, unrealistically large differences in crystal field splitting parameters (Dq).

Comparative optical absorption spectra of octahedrally coordinated Mn^{2+} in minerals

Polarized optical absorption spectra of the carbonate rhodochrosite (Fig. 3) show simple structures comprising two intense and sharp bands at 29 160 and 24 540 cm^{-1}, which mark the field-independent spin-forbidden transitions $^6A_1(S) \rightarrow {}^4E_g(D)$ and $^6A_1(S) \rightarrow {}^4E_g{}^4A_{1g}(G)$ in octahedrally coordinated Mn^{2+}. In addition, the three field-dependent bands caused by the $^6A_1(S) \rightarrow {}^4T_{2g}(D)$, $^6A_1(S) \rightarrow {}^4T_{2g}(G)$, and $^6A_1(S) \rightarrow {}^4T_{1g}(G)$ transitions in octahedrally coordinated Mn^{2+} occur at 27 620, 22 540, and 18 240 cm^{-1}. This simple Mn^{2+}-band spectrum is in keeping with the simple structure of rhodochrosite, which comprises only one regular octahedral site with all Mn-O distances equal to 2.193 Å (Maslen et al. 1995). The recorded band energies are in very good agreement with those determined from high-resolution spectra on $MnCO_3$ (Lohr and McClure 1968), but are distinctly lower (up to 200 cm^{-1}) than those determined by Keester and White (1968). Reasons for the higher band energies noted by the latter authors are not obvious, but may be related to different sample chemistry or spectral calibrations.

Distinct differences are observed in the present polarized absorption spectra of single crystals of Mn-rich forsterite and tephroite (Fig. 4). The spectra of Mn-rich forsterite show sharp bands caused by the spin-forbidden field-independent transi-

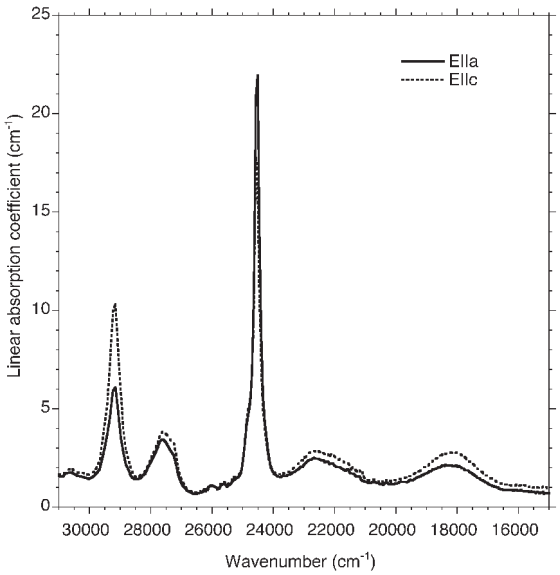

FIGURE 3. Polarized optical absorption spectra of rhodochrosite.

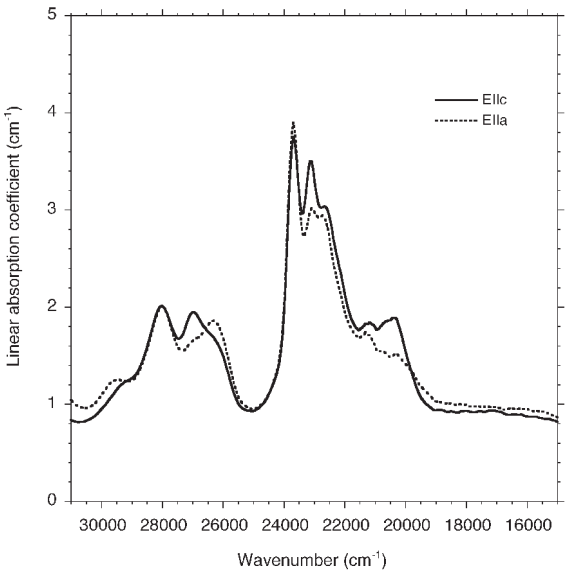

FIGURE 2. Polarized optical absorption spectra of Mn-bearing willemite.

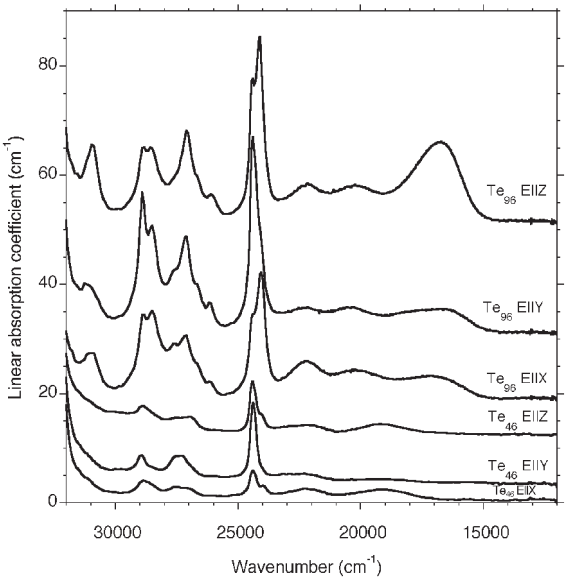

FIGURE 4. Polarized optical absorption spectra of a Mn-rich forsterite (Te_{46}) and tephroite (Te_{96}). For the sake of clarity, spectra are offset.

tions $^6A_1(S) \rightarrow {}^4E_g(D)$ and $^6A_1(S) \rightarrow {}^4E_g{}^4A_{1g}(G)$ in octahedrally coordinated Mn^{2+} at 28 880 and 24 400 cm^{-1}, respectively. Weak shoulders are present ca 300 cm^{-1} below these band maxima. In spectra of tephroite, these band shoulders are intensified and appear as strong sharp bands at 28 520 and 24 090 cm^{-1}. The field-independent bands noted at higher energies in the spectra of the Mn-rich forsterite are retained in the tephroite spectra, which results in an apparent splitting of these bands (Fig. 5). The three field-dependent Mn^{2+}-bands are observed at 19 120, 22 180, and 27 530 cm^{-1} in the spectra of the Mn-rich forsterite, while three additional field-dependent bands occur at 16 760, 20 240, and 27 100 cm^{-1} in the tephroite spectra. Consequently, the strong Mn-ordering in olivine group minerals is nicely reflected in the spectra by the two fairly intense absorption bands caused by spin-forbidden transitions in Mn^{2+} at M2-octahedra in the Mn-rich forsterite and the evolution of two additional absorption bands related to Mn^{2+} at the M1-octahedron in tephroite spectra. The distinct shift of the field-independent spin-forbidden Mn^{2+}-bands toward lower energies in spectra with increasing Mn content in samples on the join forsterite–tephroite reported by Burns (1970) is not reproduced in the present spectra. This is explained by the lower spectral resolution in his spectra, which resulted in an apparent energy-shift of unresolved bands due to variations in the intensity ratio of the two band components related to Mn^{2+} at the M2 and M1-site. The very small composition driven shifts (ca. 60 cm^{-1}) of the Mn^{2+} bands related to the M1-site noted in the present spectra indicate strong structural relaxation in the olivine structure.

Discussion

Crystal field splitting and Mn-O bond covalency

Information on crystal field splitting in $Mn^{2+}$and the degree of covalency of Mn^{2+}-L bonds can be derived from absorption spectra by solving the Tanabe-Sugano equations (Lever 1968) for the five spin-forbidden Mn^{2+}-bands (ν_1–ν_5) normally observed in the UV-Visual spectral range:

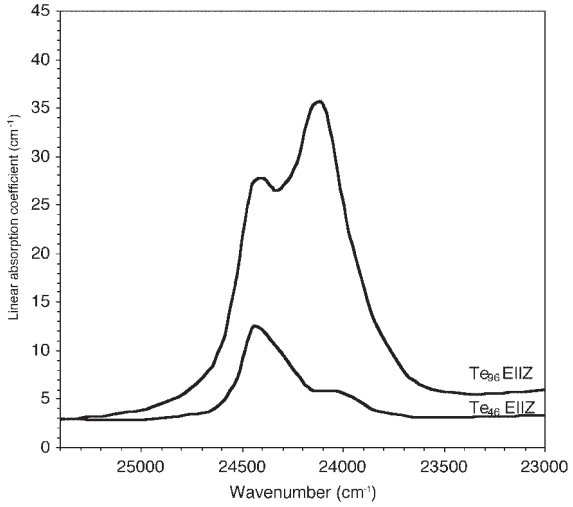

Figure 5. E||Z-spectra of the $^6A_1(S) \rightarrow {}^4E_g{}^4A_{1g}(G)$ transition in octahedrally coordinated Mn^{2+} in Mn-rich forsterite (Te_{46}) and tephroite (Te_{96}).

ν_1	$^6A_1(S) \rightarrow {}^4T_{1g}(G)$	$-10Dq + 10B + 6C - 26B^2/10Dq$
ν_2	$^6A_1(S) \rightarrow {}^4T_{2g}(G)$	$-10Dq + 18B + 6C - 38B^2/10Dq$
ν_3	$^6A_1(S) \rightarrow {}^4E_g{}^4A_{1g}(G)$	$10B + 5C$
ν_4	$^6A_1(S) \rightarrow {}^4T_{2g}(D)$	$13B + 5C + x$
ν_5	$^6A_1(S) \rightarrow {}^4E_g(D)$	$17B + 5C$

where 10 Dq is the crystal field splitting and B and C are the interelectronic repulsion Racah parameters. To fully account for electronic interactions, additional terms, as the Trees (α) and the Seniority (β) correction parameters, need to be introduced (e.g., Curie et al. 1974). In addition, access to low-temperature (below ca. 50 K) spectra providing information on the purely electronic zero phonon transitions would further improve the calculations. However, room temperature spectra in combination with the simplified expressions above may be applied for comparative semi-quantitative analyses of Me-L bonding.

Lower Dq- and B-values for tetrahedrally coordinated Mn^{2+} as compared to octahedrally coordinated Mn^{2+} is evident from Table 4, which summarizes the energies of the five Mn^{2+}-bands (ν_1–ν_5) in spectra of the present minerals and in several selected compounds from literature together with Dq-, B-, and C-values calculated by using the above expressions. The lower Dq- and B-values are consequences of lower coordination number, and thus smaller electronic Me-L repulsion, and a higher degree of bond covalency due to shorter Me-O distances in the tetrahedra. The differences are directly observed in the absorption spectra by the lower energies of the field-independent transitions (ν_5 and ν_3) and a smaller energy difference between these two bands (Δ_t) for Mn^{2+} in tetrahedral coordination (Fig. 6).

The crystal field splitting, 10Dq, for Mn^{2+} at the tetrahedral site in galaxite equals ca. 5920 cm^{-1}, which is ca. 67% of the corresponding value for octahedrally coordinated Mn^{2+} in rhodochrosite. This is in very good agreement with a theoretical value

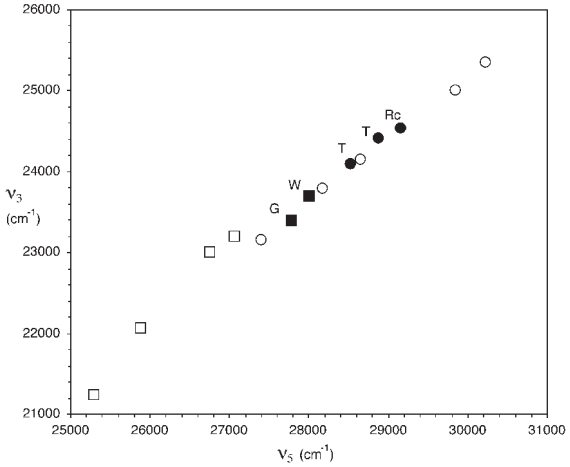

Figure 6. Plot of the energy of the $^6A_1(S) \rightarrow {}^4E_g{}^4A_{1g}(G)$ band (ν_3) vs. the energy of the $^6A_1(S) \rightarrow {}^4E_g(D)$ band (ν_5) in the Mn^{2+}-rich compounds and minerals summarized in Table 4. Squares show data for structures containing tetrahedrally coordinated Mn^{2+} and circles represent data for octahedrally coordinated Mn^{2+}. Filled symbols indicate data for the present samples, where G = galaxite, W = willemite, T = tephroite, and Rc = rhodochrosite.

TABLE 4. Mn^{2+}-bands, assignments, Racah (B and C), and crystal field splitting (Dq) parameters for divalent manganese in the present samples and in selected Mn^{2+}-rich compounds

Mineral/compound	Mn^{2+}-cluster	ν_1 (cm^{-1})	ν_2 (cm^{-1})	ν_3 (cm^{-1})	ν_4 (cm^{-1})	ν_5 (cm^{-1})	Reference	B (cm^{-1})	C (cm^{-1})	Dq (cm^{-1})
Galaxite (T-site)	MnO_4	20300	22250	23390	25970	27780	This study	627	3424	592
Willemite (T2-site)	MnO_4	21230	22700	23700	27070	28010	This study	616	3509	551
Willemite (T1-site)	MnO_4	20370	23120	23700	26320	28010	This study	616	3509	586
$MnSiN_2$	MnN_4	18380	21030	22070	24100	25890	Esmailzadeh et al. 2006	546	3323	638
ZnS:Mn	MnS_4	17891	19683	21237	22638	25297	Langer 1965	580	3087	609
$[(Me_4)N]_3[MnCl_4]$	$MnCl_4$	21200	22400	23200	26300	27070	Cotton et al. 1962	553	3534	527
$[(Et_4)N]_3[MnBr_4]$	$MnBr_4$	21350	22180	23000	25900	26750	Cotton et al. 1962	536	3529	511
Rhodochrosite	MnO_6	18240	22540	24540	27620	29160	This study	660	3588	879
Tephroite (M2-site)	MnO_6	19120	22180	24400	27530	28880	This study	640	3600	834
Tephroite (M1-site)	MnO_6	16760	20240	24090	27100	28520	This study	633	3552	1045
MnF_2	MnF_6	19440	23500	25350	28370	30230	Curie et al. 1974	697	3676	890
$Mn(ClO_4)_2{\cdot}6H_2O$	$Mn(H_2O)_6$	18690	22990	25000	27970	29850	Lohr and McClure 1968	693	3614	880
$MnSiF_6{\cdot}6H_2O$	$Mn(H_2O)_6$	18870	22990	25000	28090	29850	Lohr and McClure 1968	693	3614	869
$MnCl_2{\cdot}2H_2O$	$Mn(OH_2)_2Cl_4$	18980	21050	24130	26800	28650	Lohr and McClure 1968	646	3535	870
$[(CH_3)_4N]$ $[MnCl_3]$	$MnCl_6$	18540	22495	23785	26960	28170	Ono and Fuchikami 1977	626	3504	763
$CsMnBr_3$	$MnBr_6$	18180	21750	23150	26450	27400	McPherson et al. 1974	607	3416	745

of ca. 70%, which is based on the differences in Me-O distances in the two structures and a decreased 3d-electron repulsion (4/9 of the octahedral case) in the tetrahedron. The calculated slightly lower B-parameter, 627 cm^{-1}, for Mn^{2+} at the tetrahedral site in galaxite is in keeping with shorter Mn^{2+}-O bonds and thus a higher degree of bond covalency than for Mn^{2+} in octahedra.

Band intensity

Absorption bands caused by spin-forbidden transitions in Mn^{2+} in unbridged octahedra are generally very weak. The molar absorption coefficients (ε) recorded for such absorption bands are normally ≤0.25 L/(mol·cm) (e.g., Lohr and McClure 1968). However, magnetic coupling between structurally adjacent Mn^{2+} pairs in corner-, edge- or face-sharing octahedra has been demonstrated to result in intensified spin-forbidden absorption bands in various salts (e.g., Ferguson et al. 1965, 1966; Lohr and McClure 1968). Similar effects have been observed for spin-forbidden absorption bands in spectra of other $3d^5$-cations as, e.g., in Fe^{3+}-sulphate minerals (Rossman 1975). Absorption bands caused by spin-forbidden transitions in $3d^5$-cations in tetrahedra, which lack a center of symmetry, are expected to intensify by one to two orders of magnitude due to relaxation of the Laporte selection rule caused by mixing of p- and d-orbitals (e.g., Burns 1993).

The ε-values recorded in the present spectra for the relatively strong and sharp field-independent band caused by the $^6A_1(S) \rightarrow {}^4E_g{}^4A_{1g}(G)$ transition in octahedrally coordinated Mn^{2+} are invariably higher than those expected (Table 5). This may be caused by band intensification due to magnetically coupled Mn^{2+} pairs in corner and/or edge-sharing polyhedra in rhodochrosite and olivine group minerals (Table 6). In addition, the recorded ε-values for the M2-related field-independent band increases from 0.65 L/(mol·cm) in spectra of Mn-rich forsterite to 1.50 L/(mol·cm) in tephroite spectra (Table 5). This intensity enhancement is most likely related to transitions in coupled Mn^{2+} pairs in edge-sharing M1-M2 octahedra in tephroite. The number of such pairs is on the basis of cation occupancy determinations (Francis and Ribbe 1980) expected to be approximately one order of magnitude higher in the tephroite than in the Mn-rich forsterite.

Molar absorption coefficients for the field-independent band caused by the $^6A_1(S) \rightarrow {}^4E_g{}^4A_{1g}(G)$ transition in tetrahedrally coordinated Mn^{2+} in galaxite and Mn-bearing willemite equals 1.90 and 0.80 L/(mol·cm), respectively, which is within the range expected for normal single ion transition bands due to tetrahedrally coordinated Mn^{2+}. Considerably higher ε-values, ~50 L/(mol·cm), for the corresponding absorption band have been observed in spectra of $MnSiN_2$ (Esmaeilzadeh et al. 2006), which contain a network of magnetically ordered corner-sharing MnN_4-tetrahedra and consequently possesses a structural framework for band intensification through coupling effects. Formation of Mn^{2+} pairs in corner-sharing tetrahedra in willemite has been suggested from time-resolved photoluminescence spectra (e.g., Patra et al. 2005). Strongly intensified absorption bands caused by electronic transitions in coupled Fe^{3+} pairs in corner-sharing octahedra and tetrahedra have been observed in spectra of spinel-magnesioferrite solution crystals (Andreozzi et al. 2001). The crystal structures of galaxite and willemite contain corner-sharing cation sites (Table 6) that may facilitate pair coupling. Consequently, electronic transitions in coupled

TABLE 5. Molar absorption coefficients for the $^6A_1(S) \rightarrow {}^4E_g{}^4A_{1g}(G)$ band in the present spectra

Mineral	site	ε [L/(mol·cm)]
Galaxite	T	1.90
Willemite	T1+T2	0.80
Rhodochrosite	M	0.68
Forsterite (Te_{46})	M2	0.65
Tephroite (Te_{96})	M1	1.60
Tephroite (Te_{96})	M2	1.50

TABLE 6. Cation site sharing in the investigated minerals

Mineral	Sites	Sharing	Distance (Å)	Reference
Galaxite	T-M	corner	3.404	This study
Willemite	T1-T1	corner	3.216	Klaska et al. 1978
	T2-T2	corner	3.230	
	T1-T2	corner	3.112	
	T1-T2	corner	3.239	
Rhodochrosite	M-M	corner	3.793	Maslen et al. 1995
Forsterite	M1-M1	edge	3.062	Francis and Ribbe 1980
($Fo_{52}Te_{48}$)	M1-M2	edge	3.304	
	M1-M2	corner	3.629	
	M1-M2	corner	3,710	
	M2-M2	corner	3.936	
Tephroite	M1-M1	edge	3.117	Francis and Ribbe 1980
($Fo_{09}Te_{91}$)	M1-M2	edge	3.351	
	M1-M2	corner	3.676	
	M1-M2	corner	3.755	
	M2-M2	corner	4.009	

Mn^{2+}-pairs in galaxite and willemite as the cause for intensified optical absorption bands cannot be ruled out.

Acknowledgments

We are grateful for financial support from the Swedish Research Council (VR). We thank Sergio Lucchesi for making the single-crystal XRD facility at the University of Rome "La Sapienza" accessible. Hans Harryson, Uppsala University, is thanked for careful microprobe analytical work. Comments and suggestions by Michail Taran and an anonymous reviewer are appreciated.

References cited

Andreozzi, G.B., Hålenius, U., and Skogby, H. (2001) Spectroscopic active $^{IV}Fe^{3+}$–$^{VI}Fe^{3+}$clusters in spinel-magnesioferrite solid solution crystals: a potential monitor for ordering in oxide spinels. Physics and Chemistry of Minerals, 28, 435–444.

Bosi, F., Hålenius, U., Andreozzi, G.B., Skogby, H., and Lucchesi, S. (2007) Structural refinement and crystal chemistry of Mn-doped spinel: a case for tetrahedrally coordinated Mn^{3+} in an oxygen-based structure. American Mineralogist, 92, 27–33.

Burns, R.G. (1970) Crystal field spectra and evidence for cation ordering in olivine minerals. American Mineralogist, 55, 1608–1632.

——— (1993) Mineralogical Applications of Crystal Field Theory (2nd ed.), 551 p. Cambridge Univeristy Press, U.K.

Cotton, F.A., Goodgame, D.M.L., and Goodgame, M. (1962) Absorption spectra and electronic structure of some tetrahedral manganese (II) complexes. Journal of the American Chemical Society, 84, 167–172.

Curie, D., Barthou, C., and Canny, B. (1974) Covalent bonding of Mn^{2+} ions in octahedral and tetrahedral coordination. Journal of Chemical Physics, 61, 3048–3062.

Della Giusta, A., Carbonin, S., and Ottonello, G. (1996) Temperature-dependent disorder in a natural Mg-Al-Fe^{2+}-Fe^{3+}-spinel. Mineralogical Magazine, 60, 603–616.

Esmaeilzadeh, S., Hålenius, U., and Valldor, M. (2006) Crystal growth, magnetic and optical properties of the ternary nitride $MnSiN_2$. Chemistry of Materials, 18, 2713–2718.

Essene, E.J. and Peacor, D.R. (1983) Crystal chemistry and petrology of coexisting galaxite and jacobsite and other spinel solution and solvi. American Mineralogist, 68, 449–455

Ferguson, J., Guggenheim, H.J., and Tanabe, Y. (1965) Exchange effects in electronic absorption spectrum of Mn(2) in perovskite fluorides. Journal of Applied Physics, 36, 1046.

——— (1966) The effect of exchange interactions in the spectra of octahedral manganese II compounds. Journal of the Physical Society of Japan, 21, 1371–1385

Francis, C.A. and Ribbe, P.H. (1980) The forsterite–tephroite series: I. Crystal structure refinements. American Mineralogist, 65, 1263–1269.

Gerner, P., Fuhrer, C., Reinhard, C., and Güdel, H.U. (2004) Near-infrared to visible photon upconversion in Mn^{2+} and Yb^{3+} containing materials. Journal of Alloys and Compounds, 380, 39–44.

Greenwald, S., Pickart, S., and Grannis, F. (1954) Cation distribution and g factors of certain spinels containing Ni^{++}, Mn^{++}, Co^{++}, Al^{+++}, Ga^{+++}, and Fe^{+++}. Journal of Chemical Physics, 22, 1597–1600.

Jouini, A., Sato, H., Yoshikawa, A., Fukuda, T., Boulon, G., Kato, K., and Hanamura, E. (2006) Crystal growth and optical absorption of pure and Ti, Mn-doped $MgAl_2O_4$ spinel. Journal of Crystal Growth, 287, 313–317.

Keester, K.L. and White, W.B. (1968) Crystal field spectra and chemical bonding in manganese minerals. In P. Gay, A.F. Seager, H.F.W. Taylor, and J. Zussman, Eds., International Mineralogical association paper of the proceedings of the 5th general meeting, Cambridge, 1966, p. 22–35. Mineralogical Society, London.

Klaska, K.H., Eck, J.C., and Pohl, D. (1978) New investigation of willemite. Acta Crystallographica, B 34, 3324–3325.

Langer, D. (1965) Zero-phonon lines and phonon coupling in ZnS:Mn. Physical Review, 138, A809–A815.

Larson, A.C. (1970) The inclusion of secondary extinction in least-squares refinement of crystal structures. In F.R. Ahmed, S.R. Hall, and C.P. Huber, Eds., Crystallographic computing, p. 291–294. Munksgaard, Copenhagen.

Lavina, B., Salviulo, G., and Della Giusta, A. (2002) Cation distribution and structure modeling of spinel solid solutions. Physics and Chemistry of Minerals, 29, 10–18.

Lever, A.P.B. (1968) Inorganic electronic spectroscopy. Elsevier, Amsterdam

Lohr, L.L. and McClure, D.S. (1968) Optical spectra of divalent manganese salts II. The effect of interionic coupling on absorption strength. Journal of Chemical Physics, 49, 3516–3521

Lucchesi, S., Russo, U., and Della Giusta, A. (1997) Crystal chemistry and cation distribution in some Mn-rich natural and synthetic spinels. European Journal of Mineralogy, 9, 31–42.

Maslen, E.N., Streltsov, V.A., Streltsova, N.R., and Isgizawa, N. (1995) The electron density and optical anisotropy in rhombohedral carbonates. 3. Synchrotron X-ray studies of $CaCO_3$, $MgCO_3$ and $MnCO_3$. Acta Crystallographica, B51, 929–939.

McPherson, G.L., Aldrich, H.S., and Chang, J.R. (1974) Electronic spectrum and magnetic properties of $CsMnBr_3$. Journal of Chemical Physics, 60, 534–537.

North, A.C.T., Phillips, D.C., and Mathews, F.S. (1968) A semi-empirical method of absorption correction. Acta Crystallographica, A24, 351–359.

Ono, H. and Fuchikami, N. (1977) A calculation of magnon sideband intensities of linear chain antiferromagnet $[(CH_3)_4N][MnCl_3]$. Journal of the Physical Society of Japan, 42, 1569–1577.

Patra, A., Baker, G.A., and Baker, S.N. (2005) Effects of dopant concentration and annealing temperature on the phosphorescence from Zn_2SiO_4:Mn^{2+} nanocrystals. Journal of Luminescence, 111, 105–111.

Peacor, D.R. and Niizeki, N. (1963) The redetermination and refinement of the crystal structure of rhodonite, $(Mn,Ca)SiO_3$. Zeitschrift für Kristallographie, 119, 98–116.

Pouchou, J.L. and Pichoir, F. (1984) A new model for quantitative X-ray microanalysis. I. Application to the analysis of homogeneous samples. La Recherche Aérospatiale, 3, 13–36.

Rossman, G.R. (1975) Spectroscopic and magnetic studies of ferric iron hydroxy sulphates: intensification of color in ferric iron clusters bridged by a single hydroxide ion. American Mineralogist, 60, 698–704.

Rossman, G.R. and Taran, M.N. (2001) Spectroscopic standards for four- and five-coordinated Fe^{2+} in oxygen-based minerals. American Mineralogist, 86, 896–903.

Sreekanth Chakradhar, R.P., Nagabhushana, B.M., Chandrappa, G.T., Ramesh, K.P., and Rao, J.L. (2004) Solution combustion derived nanocrystalline Zn_2SiO_4: Mn phosphors: A spectroscopic view. Journal of Chemical Physics, 121, 10250–10259.

Taran, M.N. and Langer, K. (2001) Electronic absorption spectra of Fe^{2+} ions in oxygen-based rock-forming minerals at temperatures between 297 and 600 K. Physics and Chemistry of Minerals, 28, 199–210.

Tokonami, M. and Horiuchi, H. (1980) On the space group of spinel $MgAl_2O_4$. Acta Crystallographica, A36, 122–126.

Waychunas, G.A. and Rossman, G.R. (1983) Spectroscopic standard for tetrahedrally coordinated ferric iron-γ-$LiAlO_2$:Fe^{3+}. Physics and Chemistry of Minerals, 9, 212–215.

Manuscript received October 17, 2006
Manuscript accepted January 31, 2007
Manuscript handled by G. Diego Gatta